Large magneto-optical Kerr effect in noncollinear antiferromagnets Mn_3X (X = Rh, Ir, Pt)

Wanxiang Feng,[1,2] Guang-Yu Guo,[1,3,*] Jian Zhou,[4] Yugui Yao,[2] and Qian Niu[5,6]

[1]*Department of Physics, National Taiwan University, Taipei 10617, Taiwan*

[2]*School of Physics, Beijing Institute of Technology, Beijing 100081, China*

[3]*Physics Division, National Center for Theoretical Sciences, Hsinchu 30013, Taiwan*

[4]*Department of Materials Science and Engineering, Nanjing University, Nanjing 210093, China*

[5]*Department of Physics, The University of Texas at Austin, Austin, Texas 78712, USA*

[6]*International Center for Quantum Materials and Collaborative Innovation Center of Quantum Matter, Peking University, Beijing 100871, China*

(Received 11 August 2015; published 26 October 2015)

Magneto-optical Kerr effect, normally found in magnetic materials with nonzero magnetization such as ferromagnets and ferrimagnets, has been known for more than a century. Here, using first-principles density functional theory, we demonstrate large magneto-optical Kerr effect in high-temperature noncollinear antiferromagnets Mn_3X (X = Rh, Ir, Pt), in contrast to usual wisdom. The calculated Kerr rotation angles are large, being comparable to that of transition-metal magnets such as bcc Fe. The large Kerr rotation angles and ellipticities are found to originate from the lifting of band double degeneracy due to the absence of spatial symmetry in the Mn_3X noncollinear antiferromagnets which together with the time-reversal symmetry would preserve the Kramers theorem. Our results indicate that Mn_3X would provide a rare material platform for exploration of subtle magneto-optical phenomena in noncollinear magnetic materials without net magnetization.

DOI: 10.1103/PhysRevB.92.144426 PACS number(s): 71.15.Rf, 75.30.−m, 75.50.Ee, 78.20.Ls

I. INTRODUCTION

Magneto-optical coupling effects reflecting the interactions between light and magnetism are fundamental phenomena in solid-state physics [1]. In the nineteenth century, Faraday [2] and Kerr [3] discovered, respectively, that when a linearly polarized light beam hits a magnetic material the polarization plane of the transmitted and reflected light beams rotates. Although magneto-optical Faraday and Kerr effects have been known for over a century, they have become subjects of intense investigations only in the past decades, mainly due to the applications of optical means in modern high-density data-storage technology [4]. Faraday effect attracts less attention than Kerr effect because it can only occur in ultrathin films, where complexities of multiple reflections and discontinuous polarizations at the interfaces with the substrate arise. In contrast, magneto-optical Kerr effect (MOKE) is widely used as a powerful probe of the electronic and magnetic properties of materials, such as domain wall [5,6], surface plasma resonance [7,8], magnetic anisotropy [9,10], and topological insulator [11,12].

Band exchange splitting caused by magnetization together with relativistic spin-orbit coupling (SOC) has been recognized as the origin of MOKE [13–21]. Therefore, MOKE in various ferromagnetic transition metals as well as their alloys and compounds has been investigated extensively. By ferromagnets here we mean the magnetic materials with net magnetization including ferrimagnets. Experimentally, Erskine and Stern [14,15] first reported the MOKE spectra of bulk Fe, Co, Ni, and Gd and discussed their relationships with d bandwidths and electron-spin polarizations. After that, large Kerr rotation angles of $\sim 1.0^\circ$ were observed in several Mn-based ferromagnetic alloys, such as PtMnSb [22], MnBi [23], and $MnPt_3$ [24]. On the theoretical side, first-principles density functional calculations can directly capture the MOKE spectra with an impressive accuracy compared to experiments. For instance, Guo and Ebert [16,17] studied the MOKE spectra in bulk Fe and Co as well as their multilayers. Kim *et al.* [18] focused on the surface effect and structural dependence of the MOKE spectra in Co thin films and CoPt alloys. Stroppa *et al.* [19] analyzed the electronic structure and magneto-optical property of uniformly Mn-doped GaAs. Very recently, Rosa *et al.* [20] also investigated the magneto-optical property of Mn-doped GaAs in a special digital ferromagnetic heterostructure. Moreover, Ravindran *et al.* [21] investigated the magnetic, optical, and magneto-optical properties of manganese pnictides and found a systematic increase of the Kerr rotation angles from MnAs, to MnSb, and to MnBi.

Although MOKE experiments have been conducted on various types of ferromagnets in the past [14–24], no explicit conclusion has been established that MOKE *must be* absent when either magnetization or SOC is not present. In particular, whether MOKE can arise from a spin nonpolarized system (without magnetization) or not is still an open question. Recently, Chen *et al.* [25] showed theoretically that the anomalous Hall effect, which has a physical origin akin to that of MOKE, is large in the noncollinear antiferromagnet Mn_3Ir with zero net magnetization. This surprising result stems from the fact that in a three-sublattice kagome lattice with a noncollinear triangle antiferromagnetic configuration not only the time-reversal symmetry (TRS) $\mathcal{T}$ is broken but also there is no spatial symmetry operation $\mathcal{S}$ which, in combination with $\mathcal{T}$, i.e., the $\mathcal{TS}$, is a good symmetry that preserves the Kramers theorem. In other words, band exchange splitting exists in this system despite zero net magnetization. Naturally, it would be interesting to explore possible MOKE in Mn_3Ir as well as its isostructural materials Mn_3Rh and Mn_3Pt, which are widely considered as promising candidates in information-storage

*gyguo@phys.ntu.edu.tw

devices due to their prominent exchange-bias properties [26] and high Néel temperatures [27–29].

In this paper, we present a comprehensive first-principles study of MOKE in spin nonpolarized systems, focusing on antiferromagnets Mn_3X (X = Rh, Ir, Pt) in two low-energy noncollinear spin structures. We show that, because of the strong SOC and the breaking of band double degeneracy, the absorption rates of left- and right-circularly polarized lights differ significantly, giving rise to a previously undetected MOKE in these antiferromagnets without net magnetization. The Kerr rotation angles of Mn_3X increase from X = Rh to Ir, and to Pt, due to the increased SOC strength of the X atom. The largest one of $\sim 0.6^\circ$ in Mn_3Pt is comparable to those of elemental transition metals, such as Fe and Co, reported previously [16,17]. Our first-principles calculations also show that the MOKE would vanish if the SOC is switched off, demonstrating the essential role of the SOC for the occurrence of MOKE in these systems. Our theoretical results suggest noncollinear antiferromagnets Mn_3X to be an interesting material platform for further studies of novel magneto-optical phenomena and technological applications.

II. THEORY AND COMPUTATIONAL DETAILS

MOKE generally refers to the change in the polarization property of light when it interacts with magnetism, that is, a linearly polarized light shone on the surface of a magnetic sample will become elliptically polarized in the reflected beam. The ellipticity ϵ_K and Kerr angle θ_K (rotation of the major axis relative to the polarization axis of the incident beam) are widely used to probe and characterize magnetic materials. ϵ_K and θ_K are usually combined into the complex Kerr angle, $\phi_K = \theta_K + i\epsilon_K$. Depending on the directions of photon propagation and magnetization vector with respect to the surface plane, there are three different geometries of the Kerr effect, namely, the polar, longitudinal, and transverse geometries. Of these, the polar geometry has the largest complex Kerr angle and thus is the most interesting one in connection with technological applications. In this paper, we consider the polar geometry as a prototype and the other two geometries can be obtained similarly.

For a solid with at least threefold rotational symmetry, the elements of the optical conductivity tensor satisfy $\sigma_{xx} = \sigma_{yy}$ and $\sigma_{xy} = -\sigma_{yx}$. In such a case, the absorptive parts of the optical conductivity tensor (real diagonal and imaginary off-diagonal elements) due to interband transitions can be obtained using Kubo's formula within linear response theory [30–32]:

$$\sigma^1_{xx}(\omega) = \frac{\lambda}{\omega}\sum_{\boldsymbol{k},jj'}[|\Pi^+_{jj'}|^2 + |\Pi^-_{jj'}|^2]\delta(\omega - \omega_{jj'}), \quad (1)$$

$$\sigma^2_{xy}(\omega) = \frac{\lambda}{\omega}\sum_{\boldsymbol{k},jj'}[|\Pi^+_{jj'}|^2 - |\Pi^-_{jj'}|^2]\delta(\omega - \omega_{jj'}), \quad (2)$$

where $\lambda = \frac{\pi e^2}{2\hbar m^2 V}$ is a material specific constant, $\hbar\omega$ is the photon energy, $\hbar\omega_{jj'}$ is the energy difference between the occupied and unoccupied bands at the same $\boldsymbol{k}$ point, and $\Pi^{\pm}_{jj'} = \langle \mathbf{k}j|\frac{1}{\sqrt{2}}(\hat{p}_x \pm i\hat{p}_y)|\mathbf{k}j'\rangle$ are the dipole matrix elements for circularly polarized light with + and − helicity, respectively. The corresponding dispersive parts, namely, the imaginary diagonal element $\sigma^2_{xx}(\omega)$ and real off-diagonal element $\sigma^1_{xy}(\omega)$, can be obtained by use of the Kramer-Kronig transformation [33].

In polar geometry, the complex Kerr angle of a sample with higher than threefold rotational symmetry is simply given as [34]

$$\theta_K + i\epsilon_K = \frac{-\sigma_{xy}}{\sigma_{xx}\sqrt{1 + i(4\pi/\omega)\sigma_{xx}}}, \quad (3)$$

which can be explicitly evaluated from the optical conductivity tensor calculated from the electronic structure of the solid concerned. Since the intraband transitions contribute little to the off-diagonal elements of the optical conductivity tensor in the magnetically ordered materials [1] and affect mainly the MOKE spectra below 1–2 eV [16,17,19], here we take into account only the interband transition contribution as expressed in Eqs. (1)–(3).

In this paper, we consider ordered cubic $L1_2$ Mn_3Rh, Mn_3Ir, and Mn_3Pt alloys and adopt the experimental lattice constants of 3.813 Å [27], 3.785 Å [35], and 3.833 Å [27], respectively. The total energy and electronic structure are calculated based on first-principles density functional theory with the generalized-gradient approximation in the form of Perdew-Berke-Ernzerhof [36]. The accurate frozen-core full-potential projector augmented wave method [37], as implemented in the Vienna *ab initio* simulation package (VASP) [38,39], is used. The fully relativistic projector augmented potentials are adopted in order to include the SOC. The valence configurations of Mn, Rh, Ir, and Pt atoms taken into account in the calculations are $3d^64s^1$, $4d^85s^1$, $5d^86s^1$, and $5d^96s^1$, respectively. A large plane-wave energy cutoff of 350 eV and a fine Monkhorst-Pack $\boldsymbol{k}$-point mesh of $16 \times 16 \times 16$ are used for the self-consistent electronic structure calculations. For the calculation of optical conductivity tensors, a denser $\boldsymbol{k}$-point mesh of $20 \times 20 \times 26$ (8833 k points in the irreducible Brillouin zone) is used in the tetrahedron integration.

III. RESULTS AND DISCUSSION

In this section, we first present the calculated total energy and magnetic properties of the low-energy noncollinear magnetic structures (T1, T2, and T3) of Mn_3X (X = Rh, Ir, Pt) and also compare our results with available previous reports in Sec. III A. Then, the calculated optical conductivity, the key ingredient for evaluating the MOKE, for the two low-energy spin structures (T1 and T2) is reported in Sec. III B. Finally, we present the large magneto-optical Kerr effect in the ordered Mn_3X alloys in Sec. III C.

A. Magnetic structure

There are two kinds of crystal structures for Mn_3X alloys, namely, ordered $L1_2$ type and disordered γ phase. The ordered alloys were found to be noncollinear antiferromagnetic with one of the two nearly degenerate spin configurations, namely, the T1 and T2 triangle structures, as shown in Figs. 1(a) and 1(b), respectively. The Mn spin magnetic moments basically lie in the (111) plane and point to the center (along the edge) of the triangle, forming three nearest-neighbor Mn sublattices, for the T1 (T2) configuration, which can be

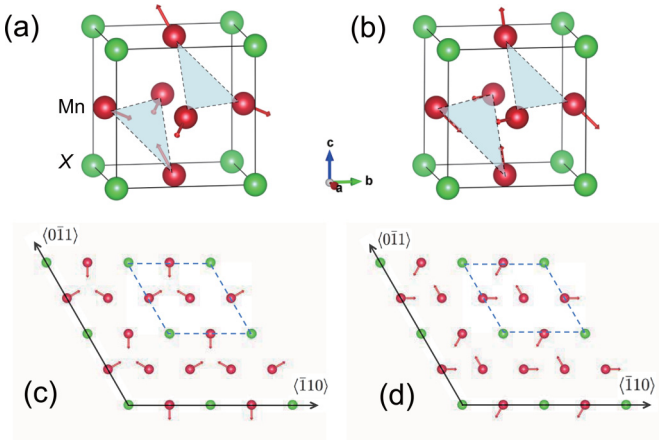

FIG. 1. (Color online) Cubic $L1_2$ crystal structure of Mn_3X (X = Rh, Ir, Pt) with (a) T1 and (b) T2 spin configurations, as well as the corresponding (111) planes in (c) and (d), respectively. The red balls (each with one arrow) and green balls (without arrow) represent Mn and X atoms, respectively. The dashed lines in (c) and (d) stand for the primitive cell of the kagome lattice.

viewed as two-dimensional kagome lattices shown in Figs. 1(c) and 1(d). Due to strong exchange interactions acting on the Mn moments, the Néel temperatures in these Mn-based alloys are as high as 475 K in Mn_3Pt [27], 855 K in Mn_3Rh [28], and 960 K in Mn_3Ir [29].

The calculated total-energy and spin magnetic moments together with previously reported experimental and theoretical results are listed in Table I. Clearly, T1 is the magnetic ground state of the Mn_3X alloys, being in good agreement with previous experimental [27] and theoretical [40] works. Nevertheless, the energy difference between the T1 and T2 spin configurations is small (being on the order of ∼1 meV), i.e., T1 and T2 are nearly degenerate. Indeed, in the absence of the SOC, all the T1, T2, and T3 spin structures have the same total energy because they are equivalent. Note that the T2 configuration here is not the same as the T2 magnetic structure reported in Ref. [40]. Our total-energy calculations show that for Mn_3Ir the total energy of the T2 structure in Ref. [40] is ∼6.4 meV higher than the T2 configuration here, and thus should be referred to as the T3 spin configuration. In the T3 configuration, the Mn magnetic moments lie along the edges of the triangles formed by three nearest-neighbor X atoms in the (111) plane [see Figs. 1(c) and 1(d), and also Fig. 5(a) in Ref. [40]].

TABLE I. The calculated total energies and spin magnetic moments for the T1, T2, and T3 magnetic structures of the Mn_3X alloys. Small total spin magnetic moments, being parallel to the ⟨111⟩ direction and due to the spin canting caused by SOC, exist. The X atoms have a zero magnetic moment, dictated by the site symmetry of their positions in the crystal structure. The available previously reported Mn spin moments are also listed for comparison. Note that the T2 structure reported in Ref. [40] is named the T3 structure here because it has a higher energy than the T2 structure here. The listed total energies are relative to that of the T1 state.

		Energy (meV)	m_{Mn} (μ_B/atom)	m_{tot} ($\langle 111\rangle_\parallel$) ($\mu_B$/cell)
Mn_3Rh	T1	0.0	3.17, 3.6,[a] 3.10,[b] 2.78[c]	0.001
	T2	0.35	3.18	0.002
	T3	1.33	3.19, 3.10[b]	0.000
Mn_3Ir	T1	0.0	2.96, 2.91,[d] 2.66,[e] 2.62[f]	0.029
	T2	2.06	2.96	0.027
	T3	8.47	2.97	0.000
Mn_3Pt	T1	0.0	3.12, 3.0,[a] 2.93[b]	0.013
	T2	0.76	3.11	0.012
	T3	2.92	3.15 2.93[b]	0.000

[a]Reference [27] (experiment).
[b]Reference [40] (theory).
[c]Reference [41] (theory).
[d]Reference [25] (theory).
[e]Reference [42] (theory).
[f]Reference [43] (theory).

The calculated spin magnetic moment of the X atom is always zero, due to its special site symmetry, while those of the Mn atoms have nearly identical values of $\sim 3\mu_B$ for all three states. The calculated spin magnetic moments agree fairly well with previous reports [25,27,40–43]. Further inspecting the total magnetization, we find a nonvanishing component along the $\langle \bar{1}\bar{1}\bar{1}\rangle$ ($\langle 111\rangle$) direction for the T1 (T2) states, because the Mn moments rotate slightly away from the (111) plane within a very small angle of ∼0.1°. Nonetheless, the Mn_3X alloys could still be considered as spin nonpolarized systems in the sense that the net total magnetization is very small and hardly affects the physical quantities of interest here, such as optical conductivities and MOKE spectra, as will be discussed in the next subsection. Note that this small spin canting is caused by the presence of the SOC. Interestingly, such a small spin canting does not occur in the T3 structure (Table I).

B. Optical conductivity

The absorptive parts of optical conductivity, i.e., σ^1_{xx} and σ^2_{xy}, have direct physical interpretations. From Eqs. (1) and (2), it is clear that σ^1_{xx} measures the average in the absorption of left- and right-circularly polarized light while σ^2_{xy} measures the corresponding difference. In Figs. 2(a) and 2(b), we show the σ^1_{xx} for the T1 and T2 spin configurations, respectively, in the energy range of 0–6 eV. Since the σ^1_{xx} is directly related to the joint density of states and interband transition probability but does not depend strongly on the details of the spin structure [19], it is not surprising that the calculated σ^1_{xx} are nearly the same for the two different spin configurations. Moreover, the σ^1_{xx} for all three Mn_3X alloys have similar behaviors, mainly due to their isostructural nature. In particular, the σ^1_{xx} for all three alloys have prominent broad peaks centered at 2.5 eV. The σ^2_{xy} for the T1 and T2 configurations are displayed in Figs. 2(c) and 2(d), respectively. For both configurations, the σ^2_{xy} of all three Mn_3X alloys have pronounced oscillatory peaks in the low-energy region and its magnitude reduces gradually to a small value above 6 eV (not shown). For each individual Mn_3X alloy, the σ^2_{xy} for the T1 and T2 states are similar in line shape and magnitude. Positive (negative) σ^2_{xy} suggests that the interband transitions are dominated by the excitations due to the left-circularly (right-circularly) polarized light. Interestingly, the sign of the σ^2_{xy} for the T1 structure can be reversed by reversing the Mn spin moments while that for the

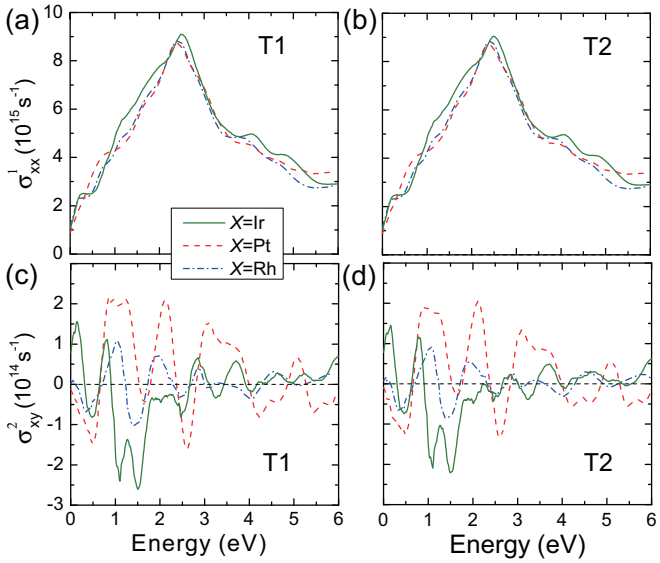

FIG. 2. (Color online) (a) and (b) The calculated real diagonal (σ^1_{xx}) as well as (c) and (d) imaginary off-diagonal (σ^2_{xy}) components of the optical conductivity tensor for the T1 and T2 spin configurations of the Mn_3X alloys. Both σ^1_{xx} and σ^2_{xy} are broadened with a Lorentzian of 0.1 eV to simulate the finite lifetime effect of electron.

T2 structure remains unchanged when the chirality of the spin structure is reversed.

The dispersive parts of optical conductivity, i.e., σ^2_{xx} and σ^1_{xy}, can be obtained from the corresponding absorptive parts by use of the Kramers-Kronig transformation. In Fig. 3, we plot the σ^2_{xx} and σ^1_{xy} for the T1 and T2 spin configurations, respectively. Figures 3(a) and 3(b) show that, similar to the σ^1_{xx}, the σ^2_{xx} are almost the same for the T1 and T2 configurations.

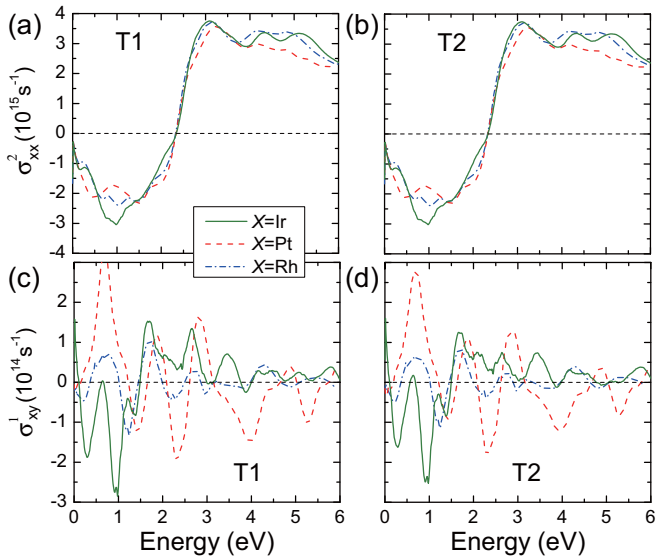

FIG. 3. (Color online) (a) and (b) The calculated imaginary diagonal (σ^2_{xx}) as well as (c) and (d) real off-diagonal (σ^1_{xy}) components of the optical conductivity tensor for the T1 and T2 spin configurations of the Mn_3X alloys. Both σ^2_{xx} and σ^1_{xy} are broadened with a Lorentzian of 0.1 eV.

The σ^2_{xx} for all Mn_3X alloys have common characteristics such as a broad valley around 1.0–1.5 eV, a negative to positive crossing point at 2.5 eV, and a broad plateau above 3.0 eV. Figures 3(c) and 3(d) show that the σ^1_{xy} spectra for the T1 and T2 configurations also have similar profiles, and gradually decay to small values in the high-energy region, which is similar to the behavior of σ^2_{xy}.

Physically speaking, the dc limit of the real part of the off-diagonal element of optical conductivity, $\sigma^1_{xy}(\omega = 0)$, is nothing but the anomalous Hall conductivity [44,45], which can also be precisely evaluated by the integration of the Berry curvature over the Brillouin zone [44,46,47]. Chen *et al.* [25] recently pointed out that the anomalous Hall effect can arise from a noncollinear antiferromagnet Mn_3Ir in the T1 spin structure without net magnetization due to the absence of certain spatial symmetries. This could be understood in terms of the fact that in the kagome lattice [the (111) plane of the Mn_3X alloys, as shown in Figs. 1(c) and 1(d)] there is no spatial symmetry $\mathcal{S}$ such as mirror and rotation that in combination with the time-reversal symmetry $\mathcal{T}$ (i.e., the $\mathcal{ST}$) can be a good symmetry such that the band Kramers degeneracy will be kept in the system with broken TRS. This is certainly in contrast to the case of, e.g., a collinear bipartite antiferromagnet, where the combination of the translational operation of half of a lattice vector with the time-reversal operation is a good symmetry that will preserve the band Kramers degeneracy despite the broken TRS due to the antiferromagnetism. This lifting of the band Kramers degeneracy together with the strong SOC in the Mn_3X alloys gives rise to the nonzero anomalous Hall conductivity. Similarly, one can expect that the σ_{xy} at optical frequencies would be nonzero as well and from Eq. (3) result in nontrivial magneto-optical Kerr effect in the Mn_3X alloys, which will be discussed in the next subsection. Of course, one may argue that the nonzero σ^2_{xy} and σ^1_{xy} could be due to the nonzero total spin magnetic moment in the T1 and T2 spin structures (Table I). To clarify this, we also calculate the σ^2_{xy} spectrum from the electronic structure with a zero spin magnetic moment obtained by forcing all the Mn moments lying in the (111) plane, and the calculated σ^2_{xy} spectrum (not shown here) is nearly identical to that obtained without fixing the Mn moments to lie in the (111) plane.

C. Magneto-optical Kerr effect

After discussing the magnetic and optical properties of the Mn_3X alloys, we now turn our attention to their magneto-optical property. From the complex Kerr angle spectra presented in Fig. 4, one can find their key features as follows.

(1) The calculated Kerr rotation angles (θ_K) and ellipticities (ϵ_K) for the T1 and T2 states have the same signs, inheriting from the behaviors of the off-diagonal elements of optical conductivity, σ^1_{xy} [see Figs. 3(c) and 3(d)] and σ^2_{xy} [see Figs. 2(c) and 2(d)].

(2) The sign reversals of θ_K and ϵ_K are frequent in the given energy range. When ϵ_K crosses the zero line, a peak turns up in the corresponding θ_K spectrum, and vice versa, which may be ascribed to the Kramers-Kronig relation.

(3) The overall features and maximum values of θ_K and ϵ_K have a size sequence of $Mn_3Pt > Mn_3Ir > Mn_3Rh$,

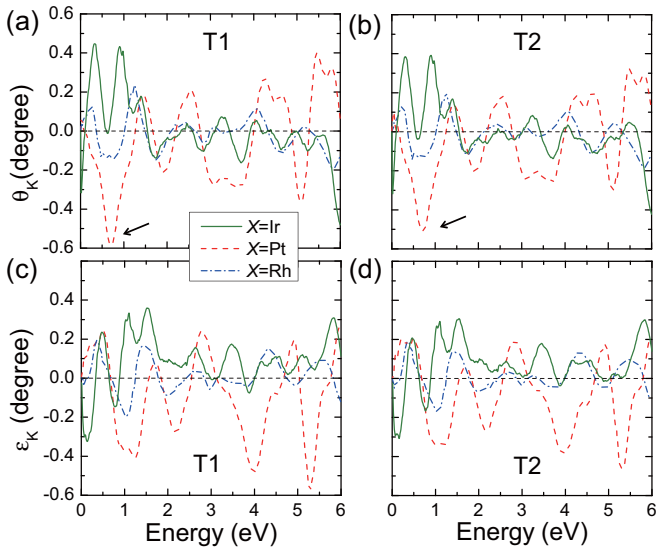

FIG. 4. (Color online) The calculated complex Kerr angles for the T1 (left panels) and T2 (right panels) spin configurations of the Mn_3X alloys: Kerr rotations (upper panels) and Kerr ellipticities (lower panels). The arrows indicate the largest Kerr rotation angles.

which suggests that the SOC strength of the X atom contributes significantly to the enhancement of the MOKE spectra.

(4) The largest Kerr rotation angle that appears in Mn_3Pt is $\sim 0.6^\circ$ at an incident photon energy of 0.7 eV. This angle arising from a noncollinear antiferromagnet is remarkably large and comparable to those of transition metals, such as the bulk and multilayers of Fe and Co studied earlier [16,17].

Finally, let us analyze the origin of the large MOKE in the Mn_3X alloys. Equation (3) indicates that a peak in a Kerr spectrum could stem from either a small σ_{xx} in the denominator or a large σ_{xy} in the numerator, which are called the "optical" and "magneto-optical" origins, respectively. From Figs. 3(c) and 4(a), one can observe that the positions of the peaks of σ^1_{xy} and θ_K for the T1 state overlap with each other, such as the first peak at 0.7 eV in Mn_3Pt and the twin peaks in the low-energy range of 0–1.0 eV in Mn_3Ir, and the same can be seen for the T2 state by comparing Figs. 3(d) and 4(b). Furthermore, the positions of the peaks of ϵ_K and σ^2_{xy} are close, as shown in Figs. 2(c) and 2(d) as well as Figs. 4(c) and 4(d), respectively. However, the magnitudes of the peaks of θ_K and ϵ_K are modulated by the σ_{xx}, as shown in Figs. 2(a) and 2(b) as well as Figs. 3(a) and 3(b), respectively. Since the Kerr rotation angle and also the ellipticity entangle in a complicated way with both the real and imaginary components of the optical conductivity tensor, there are no analytic forms for strictly separating the "optical" and "magneto-optical" origins for them. On the other hand, the nonzero σ_{xy} is clearly the fundamental cause for the emergence of the Kerr effect in this kind of noncollinear antiferromagnets, as already discussed in the preceding subsection. This is corroborated by our test calculations which show that both the σ_{xy} and MOKE in these antiferromagnets would become zero without the SOC included. Therefore, it can be concluded that the large MOKE in the Mn_3X alloys has a "magneto-optical" origin rather than the "optical" origin.

IV. SUMMARY

In conclusion, using first-principles density functional calculations, we have investigated possible magneto-optical Kerr effect in noncollinear antiferromagnets Mn_3Rh, Mn_3Ir, and Mn_3Pt. We found that the Kerr rotation angle can be as large as $\sim 0.6^\circ$ in Mn_3Pt, which is comparable to that in elemental transition-metal ferromagnets such as bcc Fe. We also discussed the differences in magneto-optical responses for the T1 and T2 spin configurations. The surprisingly large magneto-optical Kerr effect in the noncollinear antiferromagnets with nearly zero magnetization is attributed to the nontrivial off-diagonal components of optical conductivity, i.e., having the so-called "magneto-optical" origin. Our results demonstrate that one cannot assume *a priori* vanishing magneto-optical Kerr effect in antiferromagnets with zero net magnetization. The large Kerr rotation angle of the Mn_3X alloys, plus their other interesting physical properties such as prominent exchange-bias properties [26] and high Néel temperatures [27–29], would make these materials an exciting platform for exploring novel information-storage devices.

ACKNOWLEDGMENTS

Q.N. and G.Y.G. thank Hua Chen and Alan MacDonald for stimulating discussions. W.F. and G.Y.G acknowledge support from the Ministry of Science and Technology, the Academia Sinica, and NCTS of Taiwan. W.F. and Y.Y. were supported in part by the MOST Project of China (Grants No. 2014CB920903 and No. 2011CBA00108), the NSF of China (Grants No. 11374033, No. 11225418, and No. 11174337), the Specialized Research Fund for the Doctoral Program of Higher Education of China (Grants No. 20121101110046 and No. 20131101120052), and the Basic Research Fund of Beijing Institute of Technology (Grant No. 20141842004). Q.N. was supported in part by DOE-DMSE (Grant No. DE-FG03-02ER45958) and the Welch Foundation (Grant No. F-1255). W.F. also acknowledges the use of the computational resources provided by the National Supercomputer Center in Tianjin.

[1] V. Antonov, B. Harmon, and A. Yaresko, *Electronic Structure and Magneto-Optical Properties of Solids* (Kluwer Academic, Dordrecht, 2004).

[2] M. Faraday, Phil. Trans. R. Soc. **136**, 1 (1846).

[3] J. Kerr, Phil. Mag. **3**, 321 (1877).

[4] M. Mansuripur, *The Physical Principles of Magneto-Optical Recording* (Cambridge University, New York, 1995).

[5] W. Jiang, P. Upadhyaya, Y. Fan, J. Zhao, M. Wang, L.-T. Chang, M. Lang, K. L. Wong, M. Lewis, Y.-T. Lin, J. Tang, S. Cherepov, X. Zhou, Y. Tserkovnyak, R. N. Schwartz, and K. L. Wang, Phys. Rev. Lett. **110**, 177202 (2013).

[6] W. Jiang, Y. Fan, P. Upadhyaya, M. Lang, M. Wang, L.-T. Chang, K. L. Wong, J. Tang, M. Lewis, J. Zhao, L. He, X. Kou, C. Zeng, X. Z. Zhou, R. N. Schwartz, and K. L. Wang, Phys. Rev. B. **87**, 014427 (2013).
[7] V. G. Kravets, L. V. Poperenko, I. V. Yurgelevych, and D. Yu. Manko, J. Magn. Magn. Mater. **290**, 562 (2005).
[8] I. Razdolski, D. G. Gheorghe, E. Melander, B. Hjörvarsson, P. Patoka, A. V. Kimel, A. Kirilyuk, E. Th. Papaioannou, and Th. Rasing, Phys. Rev. B **88**, 075436 (2013).
[9] A. Lehnert, S. Dennler, P. Błoński, S. Rusponi, M. Etzkorn, G. Moulas, P. Bencok, P. Gambardella, H. Brune, and J. Hafner, Phys. Rev. B **82**, 094409 (2010).
[10] W. He, H.-L. Liu, H.-Y. Wu, J.-W. Cai, and Z.-H. Cheng, Appl. Phys. Lett. **106**, 042401 (2015).
[11] W.-K. Tse and A. H. MacDonald, Phys. Rev. Lett. **105**, 057401 (2010).
[12] R. Valdes Aguilar, A. V. Stier, W. Liu, L. S. Bilbro, D. K. George, N. Bansal, L. Wu, J. Cerne, A. G. Markelz, S. Oh, and N. P. Armitage, Phys. Rev. Lett. **108**, 087403 (2012).
[13] P. N. Argyres, Phys. Rev. **97**, 334 (1955).
[14] J. L. Erskine and E. A. Stern, Phys. Rev. Lett. **30**, 1329 (1973).
[15] J. L. Erskine and E. A. Stern, Phys. Rev. B **8**, 1239 (1973).
[16] G. Y. Guo and H. Ebert, Phys. Rev. B **50**, 10377 (1994).
[17] G. Y. Guo and H. Ebert, Phys. Rev. B **51**, 12633 (1995).
[18] M. Kim, A. J. Freeman, and R. Q. Wu, Phys. Rev. B **59**, 9432 (1999).
[19] A. Stroppa, S. Picozzi, A. Continenza, M. Y. Kim, and A. J. Freeman, Phys. Rev. B **77**, 035208 (2008).
[20] P. Rosa, D. Sangalli, G. Onida, and A. Debernardi, Phys. Rev. B **91**, 075207 (2015).
[21] P. Ravindran, A. Delin, P. James, B. Johansson, J. M. Wills, R. Ahuja, and O. Eriksson, Phys. Rev. B **59**, 15680 (1999).
[22] P. G. van Engen, K. H. J. Buschow, R. Jongebreur, and M. Erman, Appl. Phys. Lett. **42**, 202 (1983).
[23] G. Q. Di, S. Iwata, S. Tsunashima, and S. Uchiyama, J. Magn. Magn. Mater. **104**, 1023 (1992).
[24] T. Kato, H. Kikuzawa, S. Iwata, S. Tsunashima, and S. Uchiyama, J. Magn. Magn. Mater. **140**, 713 (1995).
[25] H. Chen, Q. Niu, and A. H. MacDonald, Phys. Rev. Lett. **112**, 017205 (2014).
[26] A. Kohn, A. Kovacs, R. Fan, G. J. McIntyre, R. C. C. Ward, and J. P. Goff, Sci. Rep. **3**, 2412 (2013).
[27] E. Krén, G. Kádár, L. Pál, J. Sólyom, P. Szabó, and T. Tarnóczi, Phys. Rev. **171**, 574 (1968).
[28] R. Yamauchi, K. Fukamichi, H. Yamauchi, and A. Sakuma, J. Alloys Compd. **279**, 93 (1998).
[29] I. Tomeno, H. N. Fuke, H. Iwasaki, M. Sahashi, and Y. Tsunoda, J. Appl. Phys. **86**, 3853 (1999).
[30] R. Kubo, J. Phys. Soc. Jpn. **12**, 570 (1957).
[31] C. S. Wang and J. Callaway, Phys. Rev. B **9**, 4897 (1974).
[32] J. Callaway, *Quantum Theory of the Solid State* (Academic, New York, 1991).
[33] H. S. Bennett and E. A. Stern, Phys. Rev. **137**, A448 (1965).
[34] F. J. Kahn, P. S. Pershan, and J. P. Remeika, Phys. Rev. **186**, 891 (1969).
[35] T. Yamaoka, J. Phys. Soc. Jpn. **36**, 445 (1974).
[36] J. P. Perdew, K. Burke, and M. Ernzerhof, Phys. Rev. Lett. **77**, 3865 (1996).
[37] P. E. Blöchl, Phys. Rev. B **50**, 17953 (1994).
[38] G. Kresse and J. Hafner, Phys. Rev. B **47**, 558 (1993).
[39] G. Kresse and J. Furthmüller, Phys. Rev. B **54**, 11169 (1996).
[40] J. Kübler, K.-H. Höck, J. Sticht, and A. R. Williams, J. Phys. F **18**, 469 (1988).
[41] A. Sakuma, R. Y. Umetsu, and K. Fukamichi, Phys. Rev. B **66**, 014432 (2002).
[42] L. Szunyogh, B. Lazarovits, L. Udvardi, J. Jackson, and U. Nowak, Phys. Rev. B **79**, 020403 (2009).
[43] A. Sakuma, K. Fukamichi, K. Sasao, and R. Y. Umetsu, Phys. Rev. B **67**, 024420 (2003).
[44] Y. G. Yao, L. Kleinman, A. H. MacDonald, J. Sinova, T. Jungwirth, D. S. Wang, E. Wang, and Q. Niu, Phys. Rev. Lett. **92**, 037204 (2004).
[45] G. Y. Guo, Y. G. Yao, and Q. Niu, Phys. Rev. Lett. **94**, 226601 (2005).
[46] D. Xiao, M.-C. Chang, and Q. Niu, Rev. Mod. Phys. **82**, 1959 (2010).
[47] G. Y. Guo, Q. Niu, and N. Nagaosa, Phys. Rev. B **89**, 214406 (2014).